Journal of Physics B: Atomic and Molecular Physics

# Experimental study of the ionisation of atomic hydrogen by fast $H^+$ and $He^{2+}$ ions

To cite this article: M B Shah and H B Gilbody 1981 *J. Phys. B: Atom. Mol. Phys.* **14** 2361

J. Phys. B: At. Mol. Phys. **14** (1981) 2361–2377. Printed in Great Britain

# Experimental study of the ionisation of atomic hydrogen by fast $H^+$ and $He^{2+}$ ions

M B Shah and H B Gilbody

Department of Pure and Applied Physics, The Queen's University of Belfast, Belfast, Northern Ireland

Received 2 February 1981

**Abstract.** Cross sections for the ionisation of ground state hydrogen atoms by 38–1500 keV $H^+$ and 125–2200 keV $He^{2+}$ ions have been determined using a crossed-beam technique. Collision products produced in the intersection of the primary ion beam with a highly dissociated thermal energy beam of hydrogen are identified by time-of-flight spectroscopy and counted using a coincidence technique. Cross sections $\sigma(H^+)$ for proton impact, which involve much smaller uncertainties and cover a wider energy range than previous measurements, now permit an accurate assessment of the validity of the various theoretical predictions. Cross sections $\sigma(He^{2+})$ for $He^{2+}$ impact, the first such measurements, are also compared with theory and measured cross section ratios $\sigma(He^{2+})/\sigma(H^+)$ are considered in terms of the $Z^2$ scaling predicted by the Born approximation.

## 1. Introduction

The ionisation of atomic hydrogen by fast protons

$$H^+ + H(1s) \rightarrow H^+ + H^+ + e \tag{1}$$

is a process of considerable fundamental and astrophysical interest. It also has an important role in controlled thermonuclear fusion research (see for example Gilbody 1979) where reliable cross sections are required over a wide range of impact energies.

Previous experimental studies of (1) have been very limited. The first measurements by Fite *et al* (1960) were carried out in the energy range 0.04–40 keV using the modulated crossed-beam technique. Protons were arranged to intersect a thermal energy beam of highly dissociated hydrogen from a tungsten tube furnace source. By chopping the beam at a fixed frequency, signals arising from the process in question could be distinguished from those arising from collisions in the background gas by their specific frequency and phase. The measurements provided the ratio of the cross sections in H to those in $H_2$. Cross sections for (1) were determined by reference to the sum of previously measured cross sections for charge transfer and ionisation in $H^+$–$H_2$ collisions. Measurements based on the modulated crossed-beam technique have also been carried out by Gilbody and Ireland (1963) in the energy range 50–400 keV. In this case, cross sections for (1) were determined by reference to known cross sections for the ionisation of $H_2$ by proton impact.

The only other previous experimental studies of (1) due to Park *et al* (1977) were based on an analysis of the differential energy-loss spectra in the passage of protons through highly dissociated hydrogen within a tungsten tube furnace. Cross sections obtained in the energy range 25–200 keV were normalised to theoretical estimates of the cross section for excitation of the $n=2$ states of H by proton impact.

In figure 1 it can be seen that the results of these three experiments are only in very rough general accord. A precise comparison of the data is precluded by the large experimental uncertainties and the different normalisation procedures. It is also evident that these results do not permit an accurate assessment of the range of validity of the various theoretical estimates of the cross sections for (1).

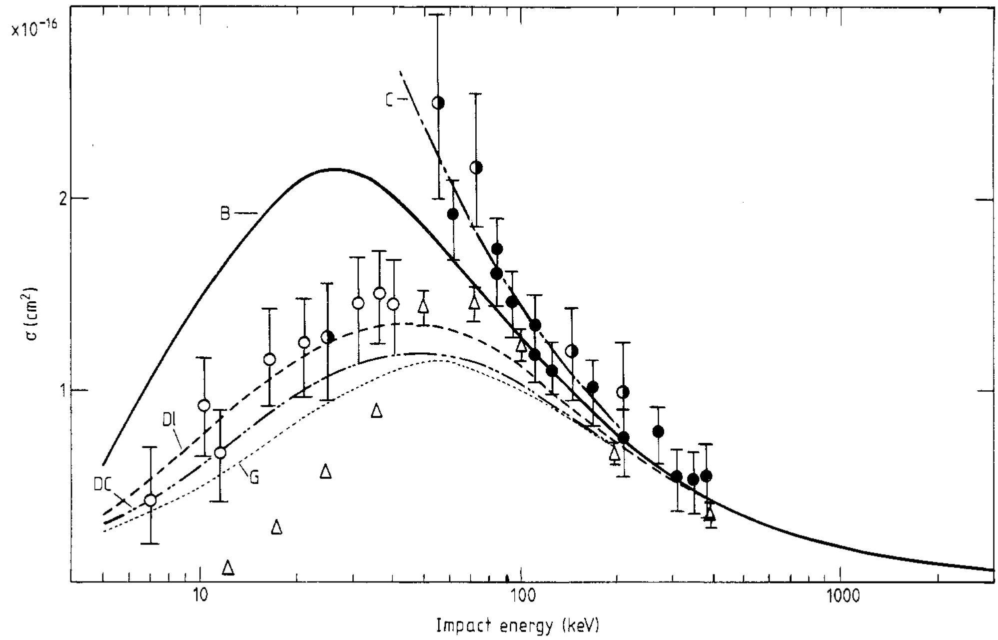


**Figure 1.** Cross sections for ionisation of H by proton impact. Experiment: ○, Fite *et al* (1960); ●, Gilbody and Ireland (1963); ◑, Park *et al* (1977). Theory: curve B, Born approximation (Bates and Griffing 1953); curve C, CDW approximation (Belkić 1978); curve G, Glauber approximation (Golden and McGuire 1975); curve DC, dipole close-coupling approximation (Janev and Presnyakov 1980); curve DI, dipole close-coupling approximation including transitions via 2p intermediate state (Janev and Presnyakov 1980); △, CTMC method (Banks *et al* 1976).

The theoretical curves shown in figure 1 are those based on the first Born approximation (Bates and Griffing 1953), the classical-trajectory Monte-Carlo method (Banks *et al* 1976), the Glauber approximation (Golden and McGuire 1975), the continuum distorted-wave approximation (Belkić 1978) and the dipole close-coupling approximation (Janev and Presnyakov 1980). These exhibit substantial differences in both magnitude and energy dependence and highlight the need for experimental cross sections of improved accuracy.

In the present work we have used a new experimental approach to obtain cross sections $\sigma(H^+)$ for (1) with greatly increased accuracy over the extended energy range 38–1500 keV. As in the previous crossed-beam measurements, a proton beam is used to intersect a thermal energy beam of highly dissociated hydrogen from a tungsten tube furnace source. However, in this work, collision products from the process in question are identified by time-of-flight analysis and counted as single particles using a coincidence technique. Our measured cross sections have been normalised to the Born approximation prediction at 1500 keV and permit an accurate assessment of the validity of this and other theoretical descriptions at lower impact energies.

We have also used the same experimental approach to obtain, for the first time, cross sections of $\sigma(He^{2+})$ for the process

$$He^{2+} + H(1s) \rightarrow He^{2+} + H^+ + e \qquad (2)$$

in the energy range 125–2200 keV. The ratio of the cross sections for (2) and (1) has been accurately determined. The relationship between these cross sections is of considerable interest in terms of the $Z^2$ scaling (where $Z$ is the projectile charge) predicted by the Born approximation.

## 2. Experimental approach

### 2.1. General description of the apparatus

A schematic diagram of the apparatus is shown in figure 2. A beam of either $H^+$ or $He^+$ ions of the required energy within the range 100–2200 keV was provided by a van de Graaff accelerator. The beam was momentum analysed by deflection in a magnetic field before passing through the 0.2 cm aperture $C_1$ prior to energy analysis by electrostatic deflection in the field provided by the plates $D_1$. The deflected beam passed through the 0.2 cm diameter apertures $C_2$ and $C_3$ which were 35 cm apart.

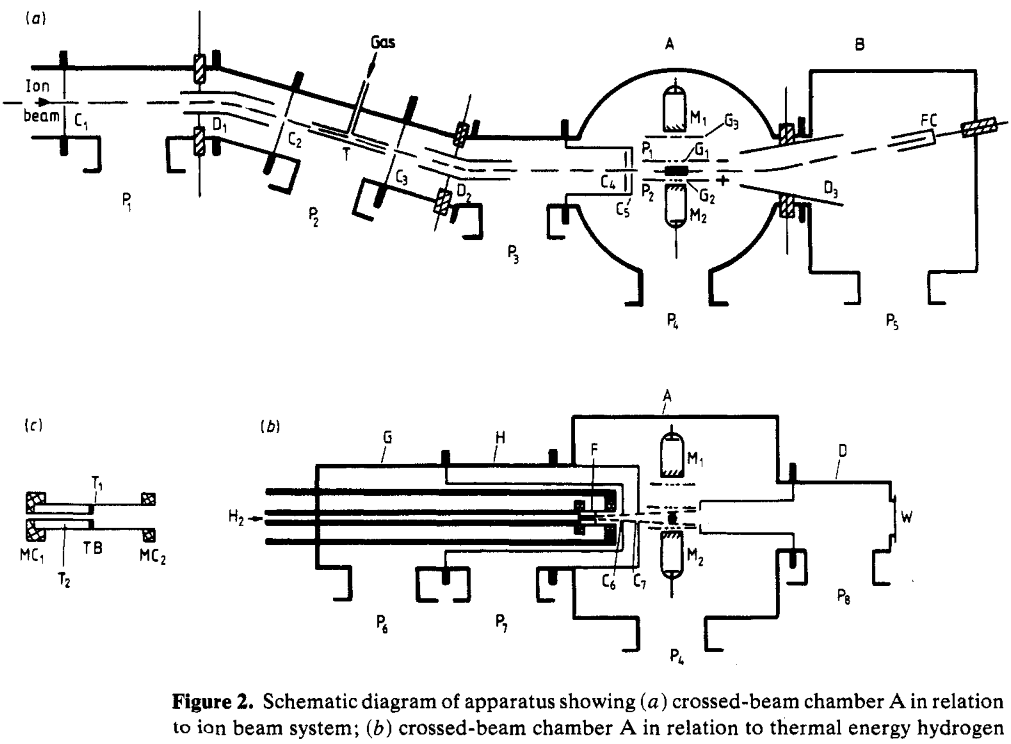


**Figure 2.** Schematic diagram of apparatus showing ($a$) crossed-beam chamber A in relation to ion beam system; ($b$) crossed-beam chamber A in relation to thermal energy hydrogen beam set at right angles to ion beam; ($c$) enlarged view of tungsten tube furnace F.

In order to produce a beam of $He^{2+}$ ions for studies of process (2), a gas-stripping canal T was located in the region between $C_2$ and $C_3$. This was 30 cm long and 2 cm in diameter and gas (usually hydrogen) was fed into the centre of T to convert a substantial fraction of a primary $He^+$ beam to $He^{2+}$ ions by charge-changing collisions. The $He^{2+}$ ions formed in this way were selected by electrostatic deflection at $D_2$.

In the measurements with fast $H^+$ ions, the gas canal T was evacuated. However, a proton beam of energy lower than about 100 keV could not be obtained directly from the van de Graaff accelerator. By passing a primary beam of $H_3{}^+$ ions through the gas-filled canal, $H^+$ break-up fragments of one third the primary beam energy could be selected by deflection at $D_2$. In this way $H^+$ beams of energy down to 38 keV were obtained. The three 4 in diffusion pumps $P_1$, $P_2$ and $P_3$ ensured that, even when gas was being admitted to T, the pressure in the regions accommodating $D_1$ and $D_2$ was maintained below $5 \times 10^{-7}$ Torr.

The beam of $H^+$ or $He^{2+}$ ions of the required energy entered the main experimental vacuum chamber A via the 0.1 cm diameter aperture $C_4$. This aperture was biased +500 V with respect to a second earthed 0.2 cm diameter aperture $C_5$ so that any secondary electrons formed at the edges of $C_4$ did not enter the main chamber.

The chamber A was 40 cm in diameter and maintained at a base pressure of about $2 \times 10^{-7}$ Torr by the 6 in diffusion pump $P_4$. A highly dissociated beam of hydrogen from a tungsten tube furnace F passed along the axis of the chamber and intersected the primary ion beam at 90°. The ion beam was then deflected electrostatically by the plates $D_3$ into the Faraday cup FC where it was recorded as a current. The chamber B which accommodated the Faraday cup was maintained at a pressure of about $2 \times 10^{-7}$ Torr by the 6 in diffusion pump $P_5$.

The tungsten tube furnace F, while utilising similar principles of construction, was rather different from the designs previously employed in this laboratory. The earlier designs used in similar experimental arrangements, produced highly dissociated beams of approximate density $10^9$ atoms/cm$^3$ in the crossed-beam intersection region. In the present design, while a high dissociation fraction was maintained, densities were increased to approximately $3 \times 10^{10}$ atoms/cm$^3$. The essential features are shown as an inset to figure 1. The main tube $T_1$ 40 mm long and 6 mm in diameter was fabricated from rolled tungsten sheet of 0.025 mm thickness. This was held and supported at each end by two molybdenum caps $MC_1$ and $MC_2$ which were housed in water-cooled copper bars connected to an AC supply. The tube was heated to the required temperature by passing a current of about 160 A through it. An inner tungsten tube $T_2$ 20 mm long and 2 mm in diameter, coaxial with $T_1$, was supported at the cold end by $MC_1$, and at the hot end by a 1 mm thick tungsten button TB. In this arrangement heating of $T_2$ takes place both by ohmic heating and by radiation from $T_1$. Hydrogen gas was passed into the inner tube $T_2$ via $MC_1$ at a steady rate from a constant pressure supply.

Highly dissociated hydrogen issuing from $T_2$ and the surrounding region of $T_1$ passed through the 0.5 cm diameter aperture $C_6$ and then through the rectangular defining slit $C_7$ located 2.0 cm beyond $C_6$. The slit $C_7$ was 0.6 cm long (in a direction parallel to the ion beam) and 0.2 cm wide. Under gas flow conditions, the pressure on the furnace side of $C_6$ was maintained at about $5 \times 10^{-5}$ Torr by the 6 in diffusion pump $P_6$ while a 4 in diffusion pump maintained the pressure in the region between $C_6$ and $C_7$ at about $6 \times 10^{-6}$ Torr. After traversing the crossed-beam intersection region which was 3.5 cm beyond $C_7$, the hydrogen beam passed into the chamber D differentially pumped by the 4 in diffusion pump $P_8$. A glass window W in the end of the chamber D allowed an optical pyrometer to be sighted on to the interior of the furnace. With a typical operating temperature of about 2600 K the useful life of the furnace before the tungsten tubes required replacement was found to be at least 50 h.

### *2.2. Signal detection*

A schematic diagram of the arrangement of the electrodes surrounding the crossed-beam intersection region is shown in figure 3. An electric field was applied across the beam intersection region by two plane grids $G_1$ and $G_2$ of 1.2 cm diameter and 90% transparency. These grids were set into plane parallel electrodes $P_1$ and $P_2$ 1.8 cm apart so that the ion beam passed mid-way between them. A negative potential was applied to $G_1$ and an equal positive potential was applied to $G_2$. Slow positive ions formed by collisions in the crossed-beam intersection region passed through $G_1$ while electrons formed as products of ionising collisions passed through $G_2$. The multipliers $M_1$ and $M_2$ (EMI type 9642/2B) were used to count the ions and electrons transmitted through $G_1$ and $G_2$. The first dynode of $M_1$ was operated at a potential of −4.5 kV while the anode was at earth potential. A high transparency grid $G_3$ in front of $M_1$ was biased at −5 kV to prevent the possible escape of secondary electrons across to $M_2$. The first dynode of $M_2$ was normally held at +1 kV while the anode was fixed at +4.5 kV.

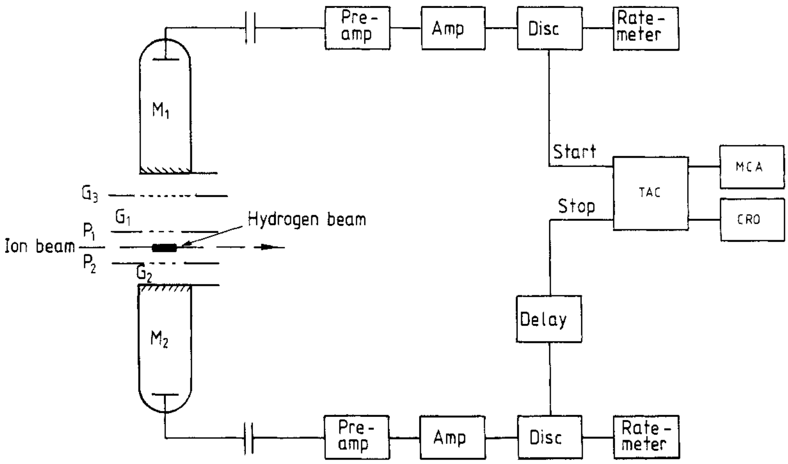


**Figure 3.** Electrode arrangement and electronics for signal recovery from crossed-beam intersection region.

The positive ions passing through $G_1$ arise from the products of ionising and charge-changing collisions between the primary ion beam and the H and $H_2$ in the target beam as well as the background gas. Product ions accelerated through the same potential difference to energies which are large compared with their initial energy spread, can be distinguished by their different times of flight to $M_1$ in accord with their charge-to-mass ratios. In this way, slow protons arising from the ionisation and charge transfer processes

$$H^+ + H \begin{array}{l} \nearrow H^+ + H^+ + e \\ \searrow H + H^+ \end{array} \qquad (3)$$

can be distinguished from $H_2^+$ ions and the various ions formed in interactions with the background gas. Furthermore, the $H^+$ ions from the ionisation channel in (3) can be selectively recorded by counting them in coincidence with the electrons from the same events. The time correlation between the $H^+$ pulses from $M_1$ and the electron pulses from $M_2$ is easily determined (see figure 3) with a time-to-amplitude converter (TAC) and recording the pulse heights in a multichannel analyser (MCA). A pulse height spectrum is then obtained in which all the product ions from each ionisation process involving H, $H_2$ and residual gases are clearly identified.

In these measurements, adequate time-of-flight mass discrimination was obtained with the separation between $G_1$ and $M_1$ set at 3.0 cm. The primary ion beam intensity was normally kept down to about $2\times10^{-11}$ A when the total ion and electron count rates from $M_1$ and $M_2$ were approximately 1000 counts/s and the coincidence count rate was about 100 counts/s. In our normal mode of operation the TAC was started by a positive ion pulse from $M_1$ and stopped by a suitably delayed electron pulse from $M_2$. A careful check was made to ensure that pulses arising from photons produced by the decay of excited species in the collision region produced no significant effects.

Figure 4 shows the dependence of the $H^+$–e coincidence count rate on the magnitude of the electric field applied between $G_1$ and $G_2$ for proton impact energies of 100 and 800 keV. In both cases, for fields of 0.83 kV cm$^{-1}$ and above, the count rate attains a constant value indicating essentially complete collection of slow ions and electrons formed in the crossed-beam intersection region. Measurements were normally carried out with the field set at 0.83 kV cm$^{-1}$. Such a field produced only a small transverse

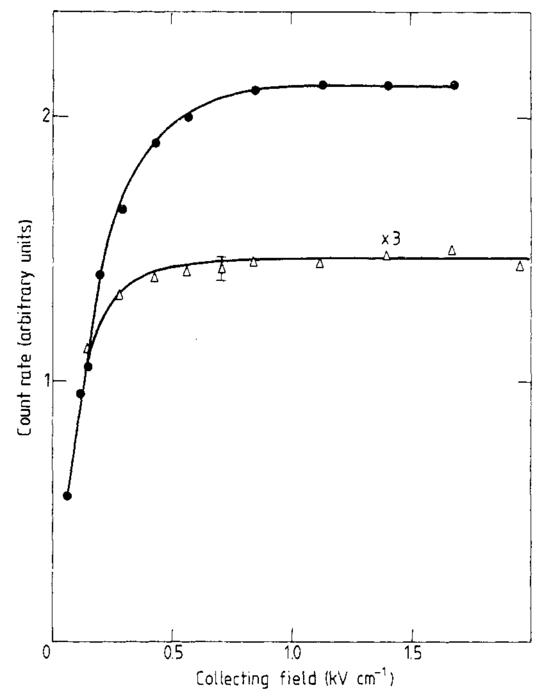


**Figure 4.** Dependence of $H^+$–e coincidence rate on collecting field applied between electrodes $G_1$ and $G_2$ of figure 3 for proton impact energies of 100 keV (●), and 800 keV (△).

deflection of the primary beam which was insufficient to significantly affect the collision geometry.

Figure 5 shows a typical pulse height spectrum obtained for proton impact in the absence of gas flow to the furnace so that, in this case, a mass spectrum corresponding to ionisation of the background gas is obtained. Peaks corresponding to the mass numbers up to about 28 are seen to be satisfactorily resolved. While the $H_2^+$ peak is negligible, a small $H^+$ peak arising from dissociative ionisation of mainly the water vapour component of the background gas is evident. The signals from water vapour and other condensible species were reduced considerably by the provision of liquid-nitrogen-cooled plates within the chamber A.

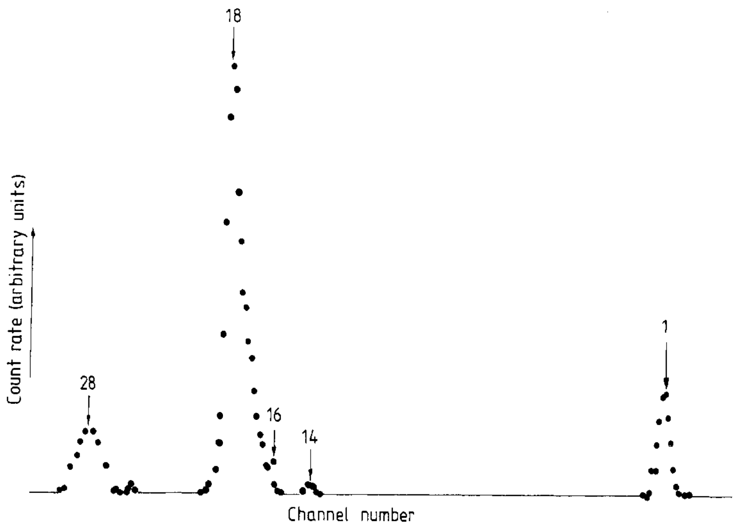


**Figure 5.** Typical pulse height spectrum corresponding to electron–ion coincidence counts obtained for protons in ionising collisions with the background gas in the absence of a hydrogen beam. Mass numbers corresponding to particular ions in the time-of-flight spectrum are indicated.

## *2.3. Signal analysis*

Figure 6 shows typical $H^+$ and $H_2^+$ signals corresponding to the electron–ion coincidence counts obtained when $H_2$ gas was fed into the furnace operated at either our standard 'low' temperature $T_0$ of 1400 K (when the beam was entirely molecular) or at a high temperature $T$ of 2600 K (when the beam was highly dissociated). It can be seen that the increase in temperature produces the expected increase in the $H^+$ signal and reduction in the $H_2^+$ signal.

The main contribution to the $H^+$–e coincidence signal arose from process (1) but proper allowance had to be made for contributions from the background gas and from dissociative ionisation of $H_2$ molecules. Apart from the undissociated $H_2$ molecules in the beam, a small increase in pressure in the chamber A, which necessarily took place when gas was admitted to the furnace, led to an extra contribution from $H_2$ molecules.

With the furnace operated at a low temperature $T_0$, the total $H^+$–e coincidence signal per unit primary ion beam current is given by

$$S_{H^+}(T_0) = S_{H^+}^{T_0}(H_2) + S_B \tag{4}$$

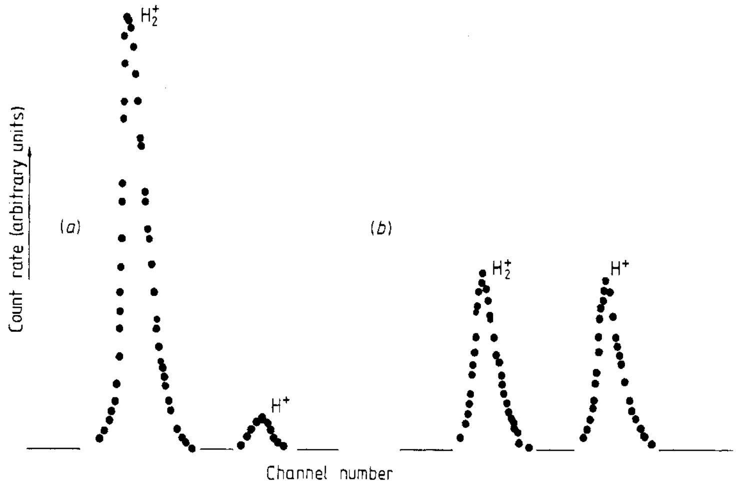


**Figure 6.** Pulse height spectra corresponding to $H^+$–e and $H_2^+$–e coincidence counts for 400 keV protons in collisions with (*a*) a beam of $H_2$ molecules from the furnace at 1400 K and (*b*) a beam of highly dissociated hydrogen from the furnace at 2600 K. Note that these signals include contributions from the background $H_2$ and residual gases (see text).

where $S_{H^+}^{T_0}(H_2)$ is the contribution arising from dissociative ionisation of $H_2$ molecules present in the beam and in the crossed-beam region. The background contribution $S_B$ arises from dissociative ionisation of residual gases (mainly $H_2O$) in the chamber and is measured in the absence of gas flow to the furnace.

When the furnace temperature is raised to $T$ while maintaining a constant rate of gas flow to the furnace, the total $H^+$–e coincidence signal per unit primary ion beam current is given by

$$S_{H^+}(T) = S_{H^+}^{T}(H) + S_{H^+}^{T}(H_2) + S_B \tag{5}$$

where $S_{H^+}^{T}(H)$ is the contribution from the H atoms in the beam and $S_{H^+}^{T}(H_2)$ is the contribution from undissociated $H_2$ molecules in the beam and in the crossed-beam region.

In table 1 we show typical values of the ratio of the background contribution $S_B$ to the total $H^+$–e coincidence count rates $S_{H^+}(T_0)$ and $S_{H^+}(T)$ observed with the furnace operated at $T_0$ and $T$ respectively. Values of $S_{H^+}(T_0)$, $S_{H^+}(T)$ and $S_B$ were assessed on the basis of five separate measurements carried out at each impact energy. In order to determine $S_{H^+}^{T}(H)$ (corresponding to the process in question) from equation (5) it is necessary to determine the contribution $S_{H^+}^{T}(H_2)$ from dissociative ionisation. This was determined by using the relation

$$S_{H^+}^{T}(H_2) = S_{H^+}^{T_0}(H_2)(S_{H_2^+}^{T}/S_{H_2^+}^{T_0}) \tag{6}$$

where $S_{H_2^+}^{T}$ and $S_{H_2^+}^{T_0}$ are the signals (based on five separate measurements) corresponding to the $H_2^+$–e coincidence channels at furnace temperatures $T$ and $T_0$ respectively. As a check on this procedure, the hydrogen background gas pressure in the chamber A was increased by a factor of about 3 so that the dissociative ionisation term became considerably larger. Within the overall experimental uncertainties, identical values were obtained for $S_{H^+}^{T}(H)$ on the basis of the expression

$$S_{H^+}^{T}(H) = S_{H^+}(T) - S_{H^+}^{T}(H_2) - S_B. \tag{7}$$

**Table 1.** Typical values of the ratio of the background contribution $S_B$ to the $H^+$–e coincidence count rates $S_{H^+}(T)$ and $S_{H^+}(T_0)$ obtained with the furnace operated at temperatures $T$ and $T_0$ respectively. The fractional contribution arising from dissociative ionisation $S^T_{H^+}(H_2)$ is also shown.

| Beam | Energy (keV) | $S_B/S_{H^+}(T_0)$ | $S_B/S_{H^+}(T)$ | $S^T_{H^+}(H_2)/S_{H^+}(T)$ |
|---|---|---|---|---|
| $H^+$ | 38 | 0.16 | 0.04 | 0.14 |
| | 400 | 0.30 | 0.05 | 0.06 |
| | 800 | 0.30 | 0.05 | 0.05 |
| | 1500 | 0.35 | 0.07 | 0.06 |
| $He^{2+}$ | 125 | 0.17 | 0.12 | 0.34 |
| | 400 | 0.21 | 0.09 | 0.19 |
| | 800 | 0.23 | 0.07 | 0.11 |
| | 2200 | 0.35 | 0.08 | 0.07 |

The fractional contribution of $S^T_{H^+}(H_2)$ to the total $H^+ + e$ count rate under typical operating conditions (table 1) is seen to be very small at high impact energies but significant at the lowest impact energies investigated, particularly in the case of $He^{2+}$ impact.

The cross section $\sigma_i$ for ionisation of H by either $H^+$ or $He^{2+}$ impact is given by

$$\sigma_i = \frac{1}{k\mu} S^T_{H^+}(H) \tag{8}$$

where $\mu$ is the effective target thickness presented by the H atoms in the beam and $k$ is a constant which reflects the efficiency of detection of the collision products. Relative values of the product $k\mu$ and hence relative cross sections for $H^+$–H collisions were determined throughout the measurements by reference to a standard proton impact energy of 400 keV. Cross sections for $He^{2+}$ impact were measured relative to those for $H^+$ by comparing signals obtained with the same hydrogen beam.

## *2.4. Normalisation procedure*

As noted in § 1, in the two previous experimental studies by Fite *et al* (1960) and Gilbody and Ireland (1963) cross sections were obtained for (1) by reference to cross sections in $H_2$ measured using the condenser plate technique. The latter involves large uncertainties, and large discrepancies are often apparent between the results of different investigators (see for example Massey and Gilbody 1974). At high velocities, condenser plate measurements in $H_2$ and the rare gases (Hooper *et al* 1962) do provide ionisation cross sections (or more correctly electron production cross sections) which are in accord with the general predictions of the Born approximation. At proton impact energies above about 500 keV, these cross sections exhibit the predicted $1/E \lg E$ energy dependence and (within the limits of experimental uncertainties) show the expected tendency to converge to corresponding cross sections for equivelocity electron impact (see Massey and Gilbody 1974). For these reasons, in the present work where our $H^+$–H cross sections extend to 1500 keV, we have normalised the relative cross sections (based on equation (8)) at our highest energies to values predicted by the first Born approximation.

It is worth noting that the first Born approximation does not provide an entirely satisfactory description of the observed double differential cross sections for electron ejection in fast proton bombardment of gas targets (Crooks and Rudd 1971). An enhanced yield of electrons, sharply peaked in the forward direction with velocities comparable to that of the primary ion, was explained by Macek (1970) in terms of electron capture to continuum states of the incoming ion. As in previous measurements, our present ionisation cross sections for (1) necessarily include, in addition to the direct proton impact ionisation, a contribution from capture into continuum states according to

$$H^+ + H(1s) \rightarrow (H^+, e) + H^+. \tag{9}$$

Theoretical and experimental estimates of cross sections for capture into continuum states (see § 3.1) indicate that there should be a negligible contribution to the measured ionisation cross sections at our highest impact velocities. Thus while the Born approximation does not take account of the contribution from (9), no appreciable error from this process should be incurred in normalising our present cross sections to the Born values at 1500 keV.

In figure 7 we show a plot of values of the product $\sigma(H^+)E$ for $H^+$–H collisions given by the Born approximation (Bates and Griffing 1953) plotted against $\lg E$. Our experimental cross sections are shown with our five highest energy values in the range 1000–1500 keV fitted to the theoretical curve. The average uncertainties of these five values reflect the uncertainty in our normalisation procedure and hence the absolute values of our cross sections. Our $H^+$-H cross sections normalised in this way thus provide values of $k\mu$ in equation (8) which are then used to determine corresponding cross sections $\sigma(He^{2+})$ for $He^{2+}$–H collisions.

Cross sections for $H^+$ and $He^{2+}$ impact are shown in table 2. Here the uncertainties associated with individual cross sections, which average ±3.5% throughout the energy range, are assessed at 90% confidence level and reflect the degree of reproducibility of the values in terms of the various experimental parameters and statistical fluctuations.

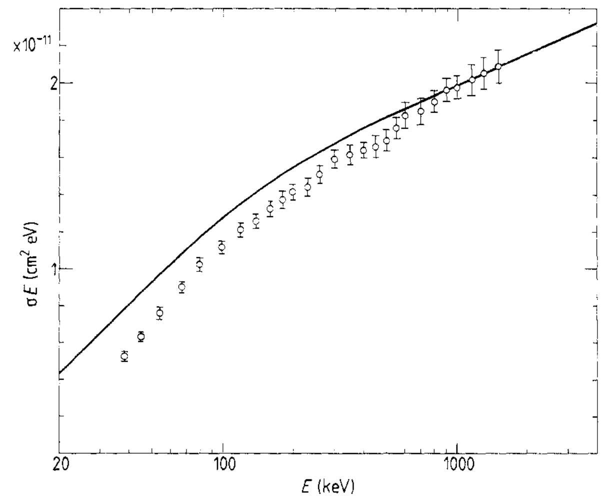


**Figure 7.** Plot of product $\sigma(H^+)E$ against lg $E$ for $H^+$–H collisions: ——, Born approximation (Bates and Griffing 1953); ○, present results normalised to Born curve at energies above 1000 keV.

**Table 2.** Ionisation cross sections for the processes $H^+ + H(1s) \rightarrow H^+ + H^+ + e$ and $He^{2+} + H(1s) \rightarrow He^{2+} + H^+ + e$.

| Energy (keV) | $\sigma(H^+)$ ($10^{-17}$ cm$^2$) | $\sigma(He^{2+})$ ($10^{-16}$ cm$^2$) |
|---|---|---|
| 38 | 13.69 ± 0.64 | — |
| 45 | 13.99 ± 0.49 | — |
| 54 | 14.04 ± 0.56 | — |
| 67 | 13.42 ± 0.43 | — |
| 80 | 12.80 ± 0.45 | — |
| 100 | 11.16 ± 0.33 | — |
| 120 | 10.09 ± 0.32 | — |
| 125 | — | 2.32 ± 0.06 |
| 140 | 8.98 ± 0.27 | — |
| 150 | — | 3.13 ± 0.10 |
| 160 | 8.27 ± 0.26 | — |
| 175 | — | 3.60 ± 0.09 |
| 180 | 7.60 ± 0.25 | — |
| 200 | 7.07 ± 0.21 | 3.89 ± 0.10 |
| 230 | 6.25 ± 0.21 | — |
| 250 | — | 4.31 ± 0.12 |
| 260 | 5.80 ± 0.19 | — |
| 300 | 5.31 ± 0.16 | 4.14 ± 0.12 |
| 350 | 4.61 ± 0.14 | — |
| 400 | 4.10 ± 0.10 | 3.80 ± 0.12 |
| 450 | 3.68 ± 0.13 | — |
| 500 | 3.38 ± 0.12 | 3.41 ± 0.11 |
| 550 | 3.19 ± 0.10 | — |
| 600 | 3.04 ± 0.12 | 3.05 ± 0.09 |
| 700 | 2.64 ± 0.11 | 2.78 ± 0.08 |
| 800 | 2.38 ± 0.07 | 2.53 ± 0.07 |
| 900 | 2.18 ± 0.07 | — |
| 1000 | 1.97 ± 0.06 | 2.16 ± 0.06 |
| 1150 | 1.75 ± 0.07 | — |
| 1200 | — | 1.89 ± 0.08 |
| 1300 | 1.58 ± 0.07 | — |
| 1400 | — | 1.70 ± 0.07 |
| 1500 | 1.39 ± 0.06 | — |
| 1600 | — | 1.55 ± 0.04 |
| 1900 | — | 1.35 ± 0.04 |
| 2200 | — | 1.18 ± 0.04 |

An additional uncertainty of ±3.8% in the $H^+$ impact cross sections is associated with our normalisation procedure. While the overall accuracy of the cross section ratios $\sigma(He^{2+})/\sigma(H^+)$ was estimated to be ±3.5%, the additional uncertainty in values of $\sigma(He^{2+})$ in table 2 is assessed at ±5.2%. The energy calibration was estimated to be within 1% and accurate checks based on observation of $p-\gamma$ resonances in $^{19}F$ were made at 340, 872 keV and (using $H_2^+$ ions) at 1744 keV.

## 3. Results and discussion

### 3.1. *Proton impact ionisation of atomic hydrogen*

Our measured cross sections $\sigma(H^+)$ for ionisation of H by protons in the range 38–1500 keV are compared with a number of theoretical predictions in figure 8. Of the previous experimental results (omitted from figure 8 in the interests of clarity), the results of Fite *et al* (1960) (figure 1) are in reasonable general accord with the low-energy trend of the present data.

As already noted, the present proton impact ionisation cross sections are normalised to the theoretical predictions of the first Born approximation (Bates and Griffing 1953) at energies in the range 1000–1500 keV. At lower impact energies, the experimental values can be seen to diverge steadily from the Born predictions and, at 38 keV, our measured cross section is only about 65% of the Born value. In addition, our measured values of $\sigma(H^+)$ attain a maximum value at about 50 keV rather than the 28 keV predicted by the Born approximation.

Golden and McGuire (1975) have used an integral representation for the scattering amplitude for ionisation by protons in the Glauber approximation which represents an improvement to the Born approximation at low and intermediate impact energies. Their predicted values of $\sigma(H^+)$ in the range 20–200 keV (figure 8) are in rather better accord with our experimental cross sections.

The classical-trajectory Monte-Carlo (CTMC) approach was first used by Abrines and Percival (1966) to describe ionisation and charge transfer in $H^+$–H collisions. The atomic electron is assumed to be moving around the nucleus in elliptical orbits and the spherically symmetric ground state of the H atom is represented by a microcanonical ensemble. The ionisation cross section at each incident proton energy is obtained by the numerical solution of the equations of motion for a three-body system. A large number of randomly selected initial trajectories must be considered to obtain results with small statistical uncertainties.

In figure 8 the values of $\sigma(H^+)$ calculated by Banks *et al* (1976) using the CTMC approach are seen to be in reasonable accord with our experimental values only at intermediate energies between about 50 and 200 keV. Below 50 keV, the CTMC values of $\sigma(H^+)$ fall much more rapidly than the observed cross sections. Above 200 keV, the CTMC values again fall more rapidly than the observed cross sections and show the expected convergence to values based on the classical impulse (binary encounter) approximation (Bates and Kingston 1970) which exhibit a $1/E$ energy dependence.

The continuum distorted-wave (CDW) approximation, originally introduced by Cheshire (1964) to describe charge transfer in $H^+$–H collisions, has been extended to the ionisation process by Belkić (1978). These calculated values of $\sigma(H^+)$ shown in figure 8 exceed measured values by about 16% at 200 keV and 104% at 40 keV.

Janev and Presnyakov (1980) have recently considered the ionisation of H by protons or multiply charged ions using the dipole approximation for the ion–atom interaction and a close-coupling method based on atomic states. They simplify the application of the close-coupling method by the introduction of an effective oscillator strength to describe the coupling of the discrete initial state with the continuum. A curve showing values of $\sigma(H^+)$ calculated in this way is shown in figure 1. A second curve also shown in figure 1, which lies between 10 and 20% higher, was obtained by taking account of transitions into the continuum via the 2p state, neglecting the contribution from other intermediate states as small. Only this second curve is shown in figure 8 where it will be seen that the agreement with our measured values of $\sigma(H^+)$ is very good down to our lowest impact energy.

As noted in § 2.4, our experimental cross sections $\sigma(H^+)$ necessarily include, in addition to direct ionisation, the contribution from capture into continuum states (process (9)). Coupled-state calculations by Shakeshaft (1978), which make use of a scaled hydrogenic basis set provide values of $\sigma(H^+)$ in the range 15–200 keV and the

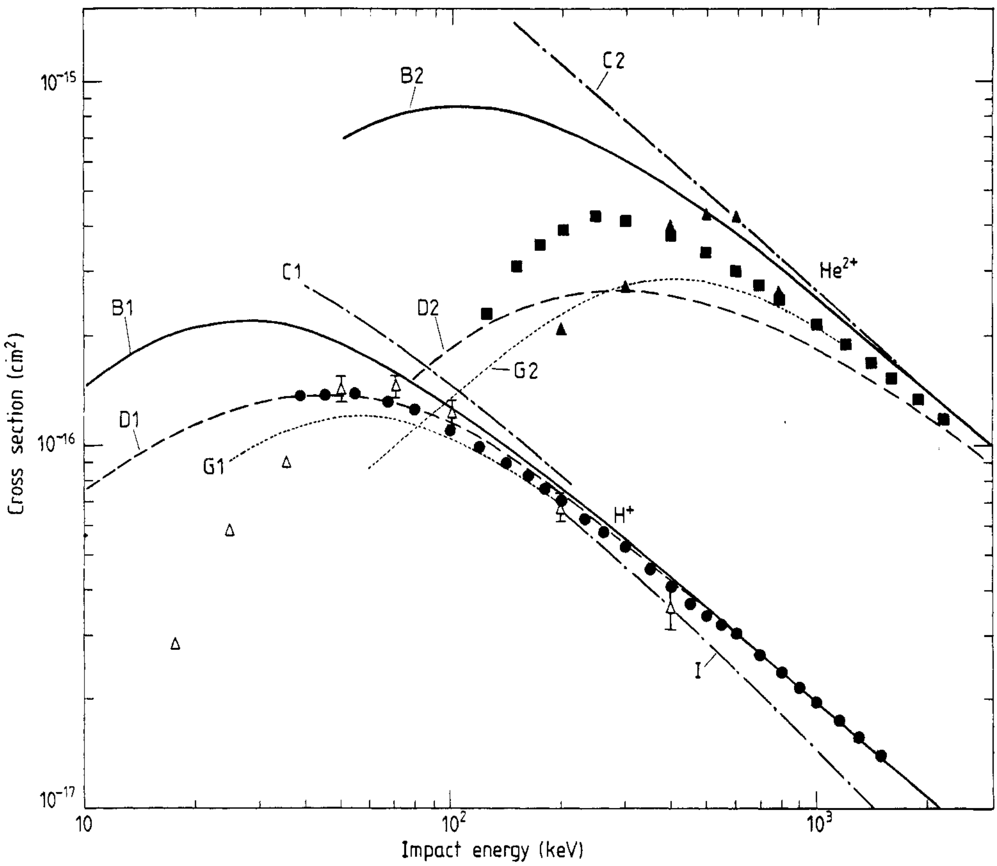


**Figure 8.** Cross sections $\sigma(H^+)$ and $\sigma(He^{2+})$ for $H^+$ and $He^{2+}$ impact ionisation of atomic hydrogen. $H^+$ impact: ●, present results: curve B1, Born approximation (Bates and Griffing 1953); curve C1, CDW approximation (Belkić 1978); curve G1, Glauber approximation (Golden and McGuire 1975); curve I, Classical impulse approximation (Bates and Kingston 1970); curve D1, dipole close-coupling approximation (Janev and Presnyakov 1980); △, CTMC method (Banks *et al* 1976). $He^{2+}$ impact: ■, present results; curve B2, Born approximation (Bates and Griffing 1953); curve C2, CDW approximation (Belkić 1980); curve G2, Glauber approximation (Golden and McGuire 1976); curve D2, dipole close-coupling approximation (Janev and Presnyakov 1980); ▲ CTMC method (Olson and Salop 1977).

separate contributions from direct ionisation and process (9). The calculated values of $\sigma(H^+)$ (see figure 9) are seen to be in good accord with our low-energy measurements. We also show the calculated contribution from (9) which, in fact, exceeds that from direct ionisation at energies below about 60 keV.

Of the other calculations so far discussed, only Banks *et al* (1976) using the CTMC method have allowed for and provided a separate estimate of the cross sections for capture into continuum states. These values (figure 9), which span the range 12.5–400 keV, are somewhat smaller than those of Shakeshaft (1978) but confirm that process (9) is very important at the lower impact energies. However, at 400 keV the contribution from (9) is seen to have decreased to about 5% of the CTMC value for $\sigma(H^+)$. A much smaller contribution from capture into continuum states is predicted by

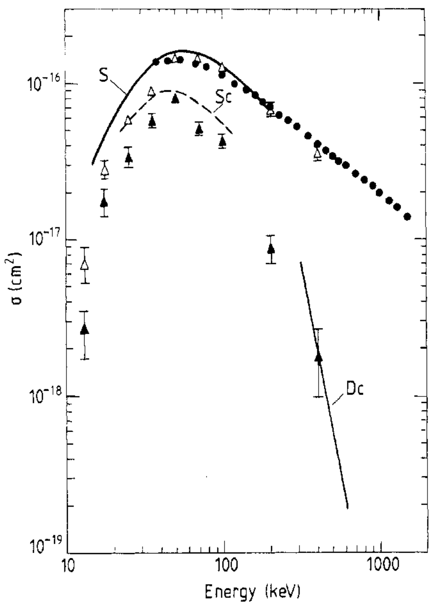


**Figure 9.** Cross sections $\sigma(H^+)$ for proton impact ionisation of H showing theoretical estimates of contribution from capture into continuum states: ●, $\sigma(H^+)$ present results; curve S, $\sigma(H^+)$ calculated by Shakeshaft (1978) with contribution from capture to continuum states shown in curve Sc; △, $\sigma(H^+)$ calculated by Banks *et al* (1976) with contribution from capture to continuum states shown ▲; curve Dc, cross sections (shown ×1000) for capture into continuum states predicted by Dettmann *et al* (1974) and Cranage and Lucas (1976).

the calculations for Dettmann *et al* (1974) using a second Born approximation. Values obtained in the range 310–609 keV shown in figure 9 exhibit an $E^{-5}$ energy dependence and are about three orders of magnitude smaller than the CTMC value at 400 keV.

Experimental cross sections for capture into continuum states measured by Cranage and Lucas (1976) for 310–609 keV protons in molecular hydrogen are a little smaller, but in reasonable general accord with values based on the calculations of Dettmann *et al* (1974). Rødbro and Andersen (1979) have also carried out an experimental study of charge transfer into the continuum for 15–1500 keV protons in a number of gases. They demonstrate the close similarity between capture to the continuum and capture to excited states and show that, at high energies, cross sections are in close accord with the theoretically predicted $E^{-5}$ energy dependence. On this basis, even if we accept the CTMC prediction for the cross section for capture into the continuum at 400 keV (figure 9), a negligible contribution to our measured ionisation cross section would be expected at our highest impact energies.

### 3.2. *$He^{2+}$ impact ionisation of atomic hydrogen*

Our measured cross sections $\sigma(He^{2+})$ for the ionisation of atomic hydrogen by $He^{2+}$ ions in the range 125–2200 keV may be compared with a number of theoretical predictions in figure 8.

At our highest impact energy of 2200 keV the measured value of $\sigma(He^{2+})$ is about 96% of the cross section predicted by the first Born approximation. At 125 keV the experimental cross section is only 27% of the Born value and the peak in the cross section is observed at about 250 keV rather than the predicted 105 keV. A less satisfactory theoretical description of $\sigma(He^{2+})$ is provided by values based on the CDW approximation (Belkić 1980) which become considerably larger than the Born cross sections at the lower impact energies.

Cross sections $\sigma(He^{2+})$ based on the Glauber approximation (Golden and McGuire 1976) are in good agreement with our measured values above about 1000 keV but become considerably smaller at lower impact energies.

Olson and Salop (1977) have used the CTMC approach to obtain values of $\sigma(He^{2+})$ which exhibit an energy dependence quite different from our measured cross sections although agreement in magnitude is observed at about 390 and 790 keV.

Cross sections $\sigma(He^{2+})$ calculated by Janev and Presnyakov (1980) using the dipole close-coupling approximation (taking account of transitions via the 2p state) agree with our measured values only at our high- and low-energy limits. While the maximum in the cross section is observed at an energy near to that predicted, the theoretical cross section is only about 64% of the measured value.

### 3.3. *Ratio of cross sections for $H^+$ and $He^{2+}$ impact*

It is well known (Bates and Griffing 1953) that cross sections for ionisation of H, obtained using the Born approximation, scale according to $Z^2$ where $Z$ is the projectile charge. Thus the Born values of $\sigma(He^{2+})$ are four times larger than $\sigma(H^+)$ for ions of the same velocity. Our measured cross section ratios $\sigma(He^{2+})/\sigma(H^+)$ which, it should be emphasised, do not rely on any normalisation procedure, permit an assessment of range of validity of the Born and other theoretical predictions.

In figure 10 the energy dependence of our measured cross section ratios $\sigma(He^{2+})/4\sigma(H^+)$ is compared with several theoretical predictions. As the particle velocity increases, the measured cross section ratio gradually approaches the (velocity-independent) value of unity predicted by the Born approximation. The measured ratio is 0.93 at our high-energy limit of 550 keV $amu^{-1}$. Below 160 keV $amu^{-1}$, ratios based on the CDW approximation can be seen to increase rapidly above the Born value whereas the experimental values decrease. The ratios based on the Glauber and dipole close-coupling approximations exhibit the correct low-velocity trend but are substantially smaller than our measured values.

Hooper *et al* (1962) have used the condenser plate technique to obtain cross sections $\sigma(H^+)$ for proton impact ionisation of molecular hydrogen in the energy range 150–1100 keV. Similar measurements have been carried out by Puckett *et al* (1969) for 200–1000 keV $He^{2+}$ ions in $H_2$. It is interesting to compare these cross sections with the present measurements in atomic hydrogen. For proton impact the cross section ratio $\sigma(H_2)/\sigma(H)$ varies from 2.07 at 150 keV to 1.74 at 1100 keV. For $He^{2+}$ impact the ratio $\sigma(H_2)/\sigma(H)$ varies from 1.59 at 200 keV to 1.93 at 1000 keV. It is also interesting to note that at 250 keV $amu^{-1}$, the highest energy at which data are available, the condenser plate measurements provide a ratio $\sigma(He^{2+})/4\sigma(H^+) = 0.92$ in $H_2$, a value which agrees exactly with our present ratio in H.

### 3.4. *Comparison with data for $H^+$–$He^+$ collisions*

It is interesting to compare the present results and their relation to theoretical predictions with corresponding data for $H^+$–$He^+(1s)$ collisions. In this laboratory

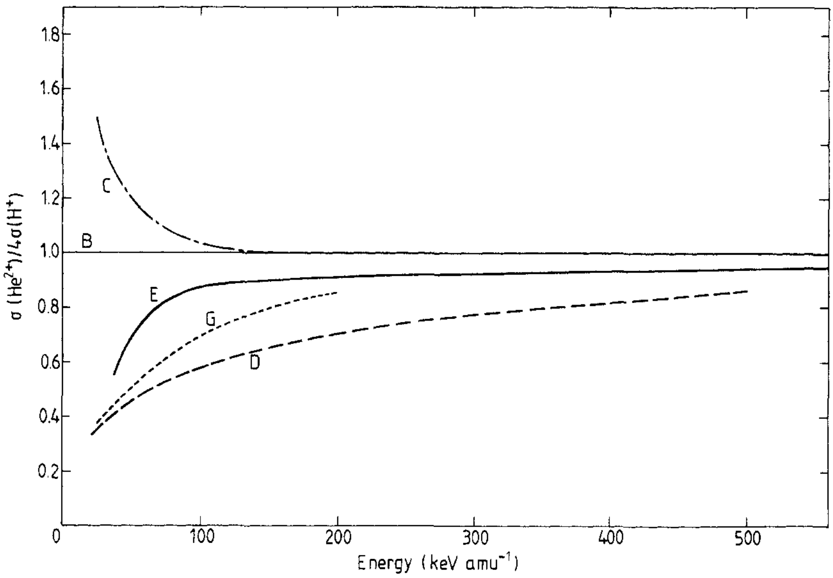


**Figure 10.** Energy dependence of cross section ratio $\sigma(He^{2+})/4\sigma(H^+)$ for particle energies expressed in keV amu$^{-1}$: curve E, present experimental results; curve B, Born approximation (Bates and Griffing 1953); curve C, CDW approximation (Belkić 1978, 1980); curve D, dipole close-coupling approximation (Janev and Presnyakov 1980); curve G, Glauber approximation (Golden and McGuire 1975, 1976).

(Angel *et al* 1978a, b) a fast intersecting-beam technique has been used to study the processes

$$H^+ + He^+(1s) \begin{array}{l} \nearrow H^+ + He^{2+} + e \\ \searrow H + He^{2+} \end{array} \qquad (10)$$

Measurements were carried out within the centre-of-mass energy range 40–386 keV and absolute cross sections $\sigma_c$ for the charge transfer process as well as the total cross section $\sigma_t = \sigma_c + \sigma_i$ for charge transfer plus ionisation were separately determined. Values of $\sigma_i = \sigma_t - \sigma_c$ were compared with theoretical values scaled from the Born values for ionisation of H by protons using the procedure set out by Bates and Boyd (1962) who show that neglect of the Coulomb repulsion between the colliding ions in (10) introduces negligible errors except at relatively low collision energies.

At their highest CM energy of 386 keV (corresponding to a laboratory energy of 482 keV for $H^+$ impact on a stationary $He^+$ ion) Angel *et al* (1978a, b) showed that the measured ionisation cross section for (10) $\sigma_i \simeq \sigma_t = 5.4 \pm 0.4 \times 10^{-18}$ cm$^2$. This value is only $79 \pm 6\%$ of the value scaled from the Born cross section for (1) at the equivalent energy of 121 keV for protons incident on H atoms (Bates and Boyd 1962). This discrepancy is not surprising in view of our present values of $\sigma(H^+)$ for (1) which, at 121 keV, are only about 83% of the Born value. In addition, we note that at 121 keV amu$^{-1}$, our measured cross section $\sigma(He^{2+})$ for ionisation of H by $He^{2+}$ ions is only about 75% of the Born cross section while our ratios $\sigma(He^{2+})/\sigma(H^+)$ confirm the inadequacy of the Born scaling procedure.

In view of their limited success in describing our measured cross sections for (1) and (2) it is perhaps not surprising that the CTMC method (Olson 1978) and the CDW approximation (Belkić 1980) provide cross sections $\sigma_i$ for (10) which are about 39% larger than the values measured by Angel *et al* (1978a, b) at 482 keV.

## Acknowledgment

The financial support of the Culham Laboratory of the United Kingdom Atomic Energy Authority is gratefully acknowledged.

*Note added in proof.* Dr J H McGuire has recently informed us that he has extended the Glauber calculation of $\sigma(H^+)$ and $\sigma(He^{2+})$ to higher velocities. While the Glauber value of $\sigma(H^+)$ is 2% smaller than the Born value of 1500 keV, the Glauber ratios $\sigma(He^{2+})/4\sigma(H^+)$ converge to our experimental ratios (figure 10) at about 450 keV $amu^{-1}$.

## References

Abrines R and Percival I C 1966 *Proc. Phys. Soc.* **88** 873–83
Angel G C, Dunn K F, Sewell E C and Gilbody H B 1978a *J. Phys. B: At. Mol. Phys.* **11** L49-53
Angel G C, Sewell E C, Dunn K F and Gilbody H B 1978b *J. Phys. B: At. Mol. Phys.* **11** L297–300
Banks D, Barnes K S and Wilson J McB 1976 *J. Phys. B: At. Mol. Phys.* **9** L141–4
Bates D R and Boyd A M 1962 *Proc. Phys. Soc.* **79** 710–6
Bates D R and Griffing G 1953 *Proc. Phys. Soc.* A **66** 961–71
Bates D R and Kingston A E 1970 *Advances in Atomic and Molecular Physics* vol 6, (New York: Academic) pp 269–318
Belkić Dž 1978 *J. Phys. B: At. Mol. Phys.* **11** 3529–52
—— 1980 *J. Phys. B: At. Mol. Phys.* **13** L589–93
Cheshire I M 1964 *Proc. Phys. Soc.* **84** 89–98
Cranage R W and Lucas M W 1976 *J. Phys. B: At. Mol. Phys.* **9** 445–54
Crooks J B and Rudd M E 1971 *Phys. Rev.* A **3** 1628–34
Dettman K, Harrison K G and Lucas M W 1974 *J. Phys. B: At. Mol. Phys.* **7** 269–87
Fite W L, Stebbings R F, Hummer D G and Brackmann R T 1960 *Phys. Rev.* **119** 663–8
Gilbody H B 1979 *Advances in Atomic and Molecular Physics* vol 15 (New York: Academic) pp 293–328
Gilbody H B and Ireland J V 1963 *Proc. R. Soc.* **277** 137–41
Golden J E and McGuire J H 1975 *Phys. Rev.* A **12** 80–4
—— 1976 *J. Phys. B: At. Mol. Phys.* **9** L11-3
Hooper J W, Harmer D S, Martin D W and McDaniel E W 1962 *Phys. Rev.* **125** 2000–4
Janev R K and Presnyakov L P 1980 *J. Phys. B: At. Mol. Phys.* **13** 4233–44
Macek J 1970 *Phys. Rev.* A **1** 235–41
Massey H S W and Gilbody H B 1974 *Electronic and Ionic Impact Phenomena* vol 4 (Oxford: Clarendon)
Olson R E 1978 *J. Phys. B: At. Mol. Phys.* **11** L227–31
Olson R E and Salop A 1977 *Phys. Rev.* A **16** 531–41
Park J T, Aldag J E, George J M and Peacher J L 1977 *Phys. Rev.* A **15** 508–16
Puckett L J, Taylor G O and Martin D W 1969 *Phys. Rev.* **178** 271–87
Rødbro M and Andersen F D 1979 *J. Phys. B: At. Mol. Phys.* **12** 2883–903
Shakeshaft R 1978 *Phys. Rev.* A **18** 1930–4